Supplemental Information

Circadian disruption worsens postseptic pulmonary fibrotic remodeling through a CLOCK/PIEZO1-linked myeloid immunometabolic program

Supplemental Materials and Methods

S1. Experimental design and sample collection

Day 0 was defined as the day of CLP or Sham surgery. CRD was initiated on postoperative day 1 and continued until the prespecified day-28 endpoint. Separate cohorts were used for circadian profiling, early molecular analyses, long-term terminal analyses, and survival monitoring. Postoperative day 3 was prespecified as the early pulmonary-injury and mechanistic endpoint, whereas postoperative day 28 was prespecified as the terminal endpoint for late fibrotic remodeling; the latter was not intended to define the onset of fibrosis.

For four-group circadian profiling, lung tissues were collected from biologically independent Sham, SALI, CRD–Sham and CRD–SALI mice (n = 6 per group at each time point) every 4 h across a 24-h cycle at ZT2, ZT6, ZT10, ZT14, ZT18 and ZT22 on postoperative day 3. For early molecular analyses, pulmonary-injury assessment and lung-macrophage flow cytometry (Figure 3, F and G), an independent cohort of animals was euthanized on postoperative day 3. Lung samples were collected for molecular analyses, Evans blue extravasation, BALF total protein concentration, lung wet-to-dry weight ratio, and arterial blood-gas analysis. For long-term fibrosis analyses shown in Figure 3, C–E and H; Supplemental Figure S3, F and G, animals surviving to the prespecified postoperative day-28 terminal collection were euthanized, and lungs were collected for histological, biochemical, and molecular measurements. The quantitative in vivo analyses shown in Figure 2, B and C and Figure 3, D, E, and G; Supplemental Figure S3G included six biologically independent mice per group. Each mouse constituted one biological replicate and one experimental unit.

The day-28 terminal cohort was distinct from the dedicated survival cohort. Survival was monitored for 28 days in the survival cohort, with 37 mice initially allocated to each group. Animals reaching a prespecified humane endpoint were euthanized and counted as deaths in the survival analysis. Such animals did not contribute to the day-28 terminal measurements. Therefore, the day-28 fibrosis-related outcomes represent survivor-conditional measurements.

S2. Survival analysis and humane endpoints

Survival was recorded daily for 28 days after CLP and analyzed using the Kaplan-Meier method with

log-rank testing. Humane endpoints included body-weight loss exceeding 20%, persistent lethargy, inability to ambulate, labored breathing, cyanosis, or gasping. Animals reaching humane endpoints were euthanized and counted as deaths in survival analyses.

S3. Histology and fibrosis assessment

At the prespecified postoperative day-28 terminal collection, surviving animals in the long-term outcome cohort were euthanized, and lung tissues were collected for fibrosis assessment. Paraffin-embedded lung sections (5 μm) were stained with H&E, Masson's trichrome, or Sirius Red using standard procedures. Fibrosis was graded using the Ashcroft score by an investigator blinded to group allocation. Fibrotic area was quantified in ImageJ from five randomly selected non-overlapping fields per section. collagen I levels in lung homogenates were measured by ELISA.

S4. Arterial blood-gas analysis

On postoperative day 3, mice were induced with 3% isoflurane and maintained with 1.5% isoflurane in room air (FiO_2 = 0.21) while breathing spontaneously without intubation or mechanical ventilation. Approximately 100 μL of arterial blood was collected from the left common carotid artery and immediately analyzed using an i-STAT 1 Analyzer (Model 300-G) with a CG8+ cartridge (Abbott Point of Care Inc., Princeton, NJ, USA).

S5. Immunofluorescence

For tissue immunofluorescence, paraffin sections were deparaffinized, rehydrated, subjected to citrate-based antigen retrieval, blocked in 5% bovine serum albumin, and incubated overnight at 4°C with primary antibodies against CD68, F4/80, Ly6G, PIEZO1, CLOCK, E-cadherin, Vimentin, α-SMA, p16, PAD4, and CitH3, followed by fluorophore-conjugated secondary antibodies. Nuclei were counterstained with DAPI. Images were acquired using a Leica SP8 confocal microscope and analyzed with Fiji/ImageJ. For cellular immunofluorescence, BMDMs, AECs, or lung fibroblasts were fixed in 4% paraformaldehyde, permeabilized with 0.1% Triton X-100, blocked, and incubated with the indicated primary antibodies. The working concentrations were 1 μg/mL BODIPY 493/503 (Invitrogen, D3922), 100 nM MitoTracker Red CMXRos (Invitrogen, M7512), 5 μM MitoSOX Red (Invitrogen, M36008) and 5 μM JC-1 (Invitrogen, T3168).

S6. Quantitative reverse-transcription PCR

Total RNA was extracted from lung tissues or cultured cells using TRIzol reagent (Invitrogen, 15596026) and

reverse-transcribed using the SuperScript III First-Strand Synthesis System (Invitrogen, 18080051). Quantitative reverse-transcription PCR was performed using SYBR Green Master Mix (Applied Biosystems, 4309155) on a QuantStudio 7 Flex Real-Time PCR System. Each biological sample was analyzed in technical triplicate, and the mean cycle-threshold value was used for subsequent calculation. Reactions (20 μL) contained 1× master mix and 300 nM of each primer. Amplification consisted of 95°C for 10 min followed by 40 cycles of 95°C for 15 s and 60°C for 1 min, with melting-curve analysis after amplification.

For all conventional mRNA-expression analyses, target-gene expression was normalized to *Gapdh* unless otherwise specified. ΔCt was calculated as: $\Delta Ct = Ct_target - Ct_Gapdh$.

For each experiment, one biologically appropriate control group was prespecified as the common calibrator. ΔΔCt was calculated as: $\Delta\Delta Ct = \Delta Ct_sample - mean\ \Delta Ct_calibrator$.

Relative mRNA expression was calculated as $2^{-\Delta\Delta Ct}$, with the mean value of the calibrator group assigned a value of 1. All genotypes and treatment groups within the same experiment were referenced to the same calibrator and were not independently rescaled. Statistical comparisons of RT–qPCR data were performed using ΔCt values, whereas the corresponding $2^{-\Delta\Delta Ct}$ values are displayed in the figures.

For Figure 2A, *Gapdh*-normalized expression values for each gene were divided by the mean value of the Sham–ZT2 group. This common normalization factor was applied to all biological samples across both groups and all time points. For the circadian analyses shown in Supplemental Figure S2, all time points and experimental groups were referenced to the Sham–ZT2 group as a single common calibrator, as specified in the figure legend. For the macrophage-abundance-adjusted analysis shown in Supplemental Figure S2F, *Gapdh*-normalized target-gene expression was additionally adjusted to *Cd14* abundance. ChIP-qPCR and mitochondrial DNA qPCR were analyzed using assay-specific normalization methods described in Sections S14 and S18. Primer sequences are listed in Supplemental Table 2. For the synchronized BMDM time-course experiments shown in Figure 7, I and J, 18S rRNA was used as the reference gene, and $2^{-}\Delta Ct$ values were used for circadian modeling without genotype-specific baseline rescaling. For Figure 4D, mRNA levels were normalized to 18S rRNA. For Supplemental Figure S4C, *Lipa* mRNA levels were normalized to *Gapdh* and expressed relative to the SALI $Piezo1^{fl/fl}$ group.

S7. Immunoblotting

Total protein was extracted from lung tissues or cultured cells using ice-cold radioimmunoprecipitation assay (RIPA) lysis buffer supplemented with protease and phosphatase inhibitors. Protein concentrations were

determined using a bicinchoninic acid assay (Pierce BCA Protein Assay Kit, Thermo Fisher Scientific, 23225). Equal amounts of protein (30 μg per lane) were separated using sodium dodecyl sulfate–polyacrylamide gel electrophoresis (SDS-PAGE) gels selected according to the molecular weight of the target protein and transferred onto polyvinylidene fluoride membranes. Protein lysates were collected on postoperative day 3 for Figure 2, B and C, from surviving animals at the postoperative day-28 terminal endpoint for Supplemental Figure S3, F and G, after 24 h of Yoda1 treatment for Figure 4, E, H, and I, after 4 h of LPS plus PMA stimulation for Figure 5, G and H, 48 h after lentiviral transduction for Figure 7, B, C, and H, and after 24 h of indirect Transwell co-culture for Figure 8, H and I; samples from the cycloheximide-chase experiments were collected at the indicated time points.

Membranes were blocked with 5% non-fat milk or 5% bovine serum albumin in Tris-buffered saline containing 0.1% Tween-20 for 1 h at room temperature and incubated with the indicated primary antibodies overnight at 4°C. After washing, membranes were incubated with the corresponding horseradish peroxidase-conjugated secondary antibodies for 1 h at room temperature. Antibody suppliers, catalog numbers, clones and dilutions are listed in Supplemental Table 3.

Protein bands were visualized using enhanced chemiluminescence. Images used for densitometric analysis were acquired within the non-saturated linear exposure range. Band intensity was quantified using ImageJ. Membranes were not stripped and reprobed. Each target protein was normalized to the loading control detected on the corresponding membrane and identical lane set. GAPDH, β-actin or β-tubulin was used as specified in the corresponding figure legend, and the complete membrane-matched loading controls are provided with the uncropped immunoblots. Quantitative data were derived from biologically independent samples rather than repeated measurements of the same lysate. Uncropped immunoblots with molecular-weight markers are provided in Supplemental information.

S8. Flow cytometry

For lung immune profiling, lungs were enzymatically dissociated, filtered, and stained with antibodies against CD45, CD11b, F4/80, CD86, and CD206. Macrophages were defined as $CD45^{+}CD11b^{+}F4/80^{+}$ cells, and CD86 and CD206 were used to assess inflammatory- and repair-associated macrophage marker profiles, rather than to assign fixed M1/M2 states. For analysis of inflammatory marker expression in BMDMs, cells were stained for surface CD11b, F4/80 and CD86, then fixed, permeabilized and stained intracellularly for CD68. The percentages of CD68-positive and CD86-positive cells were quantified among $CD11b^{+}F4/80^{+}$ gated BMDMs.

For mitochondrial oxidative stress assays, AECs were stained with MitoSOX Red and analyzed by flow cytometry.

S9. Isolation and culture of primary cells

Bone marrow-derived macrophages (BMDMs) were generated from mouse femurs and tibias in RPMI 1640 supplemented with 10% fetal bovine serum, 1% penicillin/streptomycin, and 20 ng/mL macrophage colony-stimulating factor (M-CSF; R&D Systems, 416-ML) for 7 days. BMDMs were used for the cell-based experiments in Figure 6. Alveolar macrophages (AMs) for Supplemental Figure S4 were isolated by bronchoalveolar lavage (BAL) and sorted as described below. Primary alveolar epithelial cells (AECs) were isolated from adult mouse lungs after vascular perfusion, Dispase II/agarose inflation, enzymatic dissociation, and negative selection to deplete non-epithelial cells. Cells were cultured on fibronectin-coated plates in DMEM/F12 medium. Primary mouse lung fibroblasts were isolated by explant culture in DMEM containing 20% fetal bovine serum and used between passages 2 and 5.

For the ex vivo analyses in Supplemental Figure S4, BAL cells from SALI and CRD–SALI mice of both *Piezo1* genotypes were collected, Fc-blocked and stained without fixation. Debris, doublets and dead cells were excluded, and AMs were sorted as live singlet $CD45^{+}Ly6G^{-}CD64^{+}CD11c^{hi}Siglec\text{-}F^{hi}$ cells. The sorted fraction was reanalyzed using the same phenotypic gate to assess purity and was used for *Lipa* RT–qPCR, LAL activity and intracellular TG measurements. Cells were incubated with 1 μg anti-CD16/CD32 per 10^{6} cells for 10 min at 4°C, then surface-stained for 30 min at 4°C in PBS containing 2% FBS. Fluorochromes, clones and antibody dilutions are listed in Supplemental Table 3. Post-sort purity was calculated as the percentage of AM-gated events among live singlets in the reanalyzed sorted fraction.

S10. In vitro stimulation and LAL restoration

BMDMs were synchronized in 0.5% serum for 12 h before stimulation. Cells were treated with LPS (100 ng/mL; *E. coli* O55:B5, Sigma-Aldrich, L2880), Yoda1 (10 μM; Sigma-Aldrich, SML1558), GsMTx4 (5 μM, 30 min pretreatment; Abcam, ab141871), DNase I (100 U/mL; Sigma-Aldrich, D5025), or 2-bromopalmitate (2-BP; 50–100 μM; Sigma-Aldrich, 21604) as indicated. To induce extracellular trap-like responses in BMDMs, cells were stimulated with LPS plus PMA (100 nM; Sigma-Aldrich, P1585) for 4 h unless otherwise indicated. For LAL rescue experiments, BMDMs were transduced with a lentiviral vector encoding mouse *Lipa*, and cells transduced with the corresponding empty vector served as negative controls (NC). Cells were allowed to recover

for 48–72 h and were then treated with Yoda1 for 24 h before downstream analyses. The Yoda1+LAL label denotes Yoda1-treated cells transduced with the mouse *Lipa* expression vector.

S11. Lipid metabolism and lipophagy assays

Intracellular triglycerides (Triglyceride Quantification Kit, Sigma-Aldrich, MAK266) and total free fatty acids (Free Fatty Acid Quantitation Kit, Sigma-Aldrich, MAK044) were quantified using colorimetric assays and normalized to total protein. Absorbance was measured at 570 nm. Lipid peroxidation was assessed using a 4-HNE ELISA Kit (Elabscience, E-EL-0128). For lipophagy analyses, cells were stained with BODIPY 493/503 and immunostained for LC3B or LAMP1. Colocalization between lipid droplets and autophagic or lysosomal markers was quantified in Fiji/ImageJ. Fatty acid β-oxidation was measured using [1-^{14}C]-palmitate, and oxidation rates were determined by quantifying released $^{14}CO_2$ and acid-soluble metabolites. Transcriptome profiling of Yoda1+NC and Yoda1+LAL BMDMs was used to assess pathway-level restoration of lipid-catabolic programs.

In sorted AMs, LAL activity was measured in cell lysates using 100 μM 4-methylumbelliferyl palmitate (Cayman Chemical, 16089) in sodium acetate buffer at pH 4.5 for 30 min at 37°C. Reactions were stopped by alkalinization, and fluorescence was measured at excitation/emission wavelengths of 360/460 nm using a 4-methylumbelliferone standard (Sigma-Aldrich, M1381). Paired aliquots were incubated with 30 μM Lalistat-2 (Sigma-Aldrich, SML2053). LAL activity was calculated by subtracting the inhibited from the uninhibited reaction and expressed as product formed per hour per milligram of lysate protein. Intracellular TG was measured in matched preparations using the MAK266 assay with a no-lipase blank to correct for free glycerol. Total protein was determined by BCA in a separate, assay-compatible aliquot. Protein-normalized LAL activity and TG were expressed relative to the mean of the SALI *Piezo1*$^{fl/fl}$ group. *Lipa* mRNA was analyzed by RT–qPCR as described in Section S6.

S12. MET detection and inflammatory readouts

Extracellular DNA release from BMDMs was visualized using 1 μM SYTOX Green (Invitrogen, S7020). Extracellular trap-associated markers were assessed by immunofluorescence staining for PAD4 and CitH3 and by immunoblotting for PAD4, CitH3, MPO, MMP-2, and MMP-9. For ultrastructural validation, stimulated BMDMs were processed for scanning electron microscopy. TNF-α, IL-6, and IL-1β in culture supernatants were measured by ELISA. Cell-free DNA, MPO, and macrophage elastase in human serum were quantified using the

Quant-iT PicoGreen dsDNA Assay Kit (Invitrogen, P11496) or ELISA, according to the manufacturers' protocols. PicoGreen reagent was diluted 1:200 before mixing with samples.

S13. Transwell and co-culture systems

BMDMs were stimulated as indicated to induce MET-like responses. The experimental groups comprised vehicle control, LPS, LPS plus GsMTx4, LPS plus Yoda1, and LPS plus Yoda1 and DNase I; reagent concentrations and the 30-min GsMTx4 pretreatment were as described in Section S10. DNase I was included during macrophage stimulation where indicated to digest extracellular DNA scaffolds. After stimulation, the BMDMs were thoroughly washed to remove residual reagents, transferred to fresh medium, and placed in the upper chambers of Transwell inserts, whereas purified AECs were cultured in the lower chambers. The two cell types were maintained in indirect co-culture for 24 h, after which the AECs were collected for downstream analyses. For fibroblast migration assays, washed pretreated BMDMs were placed in the lower chamber and fibroblasts in 8-μm inserts. Direct macrophage–fibroblast co-cultures were performed on glass-bottom dishes for AFM and p-MLC analyses.

S14. Cytosolic mtDNA quantification and mitochondrial assays

Total and cytosolic mtDNA in recipient AECs were quantified after digitonin-based subcellular fractionation. DNA was extracted from total lysates and cytosolic fractions, and mitochondrial DNA targets (*mt-Nd1*, *mt-Co1*, and the noncoding D-loop region) were measured by qPCR. Mitochondrial membrane potential was evaluated using JC-1 staining, and the red/green fluorescence ratio was used as an index of mitochondrial polarization. Mitochondrial ultrastructure was further examined by transmission electron microscopy after fixation, osmication, dehydration, resin embedding, and ultrathin sectioning.

S15. Palmitoylation and PAD4 stability assays

A targeted CRISPR/Cas9 loss-of-function screen against selected murine *Zdhhc* family members was performed in BMDMs to identify the palmitoyl acyltransferase responsible for PAD4 modification. Candidate effects on PAD4 palmitoylation were evaluated using alkynyl-palmitate labeling. For bio-orthogonal palmitoylation assays, cells expressing the indicated constructs were labeled with 17-ODYA (Cayman Chemical,

90270), followed by click-chemistry conjugation to biotin-azide and streptavidin enrichment. PAD4 palmitoylation was assessed by immunoblotting. For acyl-PEG exchange (APE) assays, free thiols were blocked with N-ethylmaleimide, thioester bonds were cleaved with hydroxylamine, and newly exposed cysteines were labeled with mPEG-maleimide. A mobility shift of PAD4 on immunoblots was interpreted as evidence of palmitoylation. PAD4 stability was assessed by chase assays with 50 μg/mL cycloheximide (Sigma-Aldrich, C7698) after genetic or pharmacologic inhibition of palmitoylation. Samples were collected at the time points shown in the figures. For the pharmacologic destabilization assay, 2-BP was used at 100 μM, as in the corresponding figure.

S16. Co-immunoprecipitation and in vitro palmitoylation

For co-immunoprecipitation, BMDMs expressing tagged PAD4 and ZDHHC19 were lysed, immunoprecipitated with anti-Flag or anti-SFB antibodies, and analyzed by immunoblotting. For in vitro palmitoylation, recombinant WT or mutant PAD4 and ZDHHC19 proteins were incubated with biotin-palmitoyl-CoA, and reaction products were detected by streptavidin-HRP.

S17. Molecular docking

Structural docking between ZDHHC19 and PAD4 was performed using models obtained from AlphaFold or the RCSB Protein Data Bank. Protein preparation was carried out in AutoDockTools, docking was performed in AutoDock Vina, and the lowest-energy pose was visualized in PyMOL.

S18. CLOCK-dependent transcriptional regulation of *Piezo1* in BMDMs

Mature BMDMs derived from *Clock*$^{fl/fl}$ and *Clock*$^{\Delta LysM}$ mice were transduced with a lentiviral vector expressing mouse CLOCK or the corresponding empty vector and collected 48 h later for RT–qPCR and immunoblotting, with all genotype-treatment groups processed in parallel. The mouse *Piezo1* promoter sequence was retrieved from the mm39 genome assembly and analyzed using JASPAR; a canonical E-box motif located at -654 to -649 bp relative to the transcription start site (CACGTG; E-box 1) was selected for functional analysis, whereas the -900 to -750 bp region served as a motif-negative control. For ChIP, synchronized BMDMs were collected at CT10 and CT22, cross-linked with 1% formaldehyde, and sonicated to generate 200–500 bp chromatin fragments. Chromatin was immunoprecipitated using an anti-CLOCK antibody or control IgG, with 1% retained as input, and enrichment at the E-box 1 and negative-control regions was quantified by qPCR and expressed as a percentage of input; corresponding endpoint PCR products were

visualized by 2% agarose gel electrophoresis. For reporter assays, the wild-type *Piezo1* promoter and an E-box 1-mutant promoter containing the CACGTG-to-CAAGTG substitution were cloned into a Firefly luciferase vector and sequence-verified. BMDMs were nucleofected with the reporter constructs, a Renilla control plasmid, and either the CLOCK expression plasmid or empty vector, and Firefly activity was normalized to Renilla activity and expressed relative to the wild-type promoter plus empty-vector group. For endogenous E-box 1 editing, paired sgRNAs flanking the motif were introduced as Cas9 ribonucleoprotein complexes into bone marrow-derived myeloid progenitor cells before macrophage differentiation. Editing was verified by genomic PCR, bidirectional Sanger sequencing, and ICE analysis. At least two independently generated edited pools were used, and wild-type and E-box 1-edited BMDMs were subsequently transduced with CLOCK or empty vector and collected 48 h later for RT–qPCR and immunoblotting.

S19. BMDM synchronization and circadian rhythm analysis

Mature BMDMs were adapted in medium containing 0.5% serum for 12 h and synchronized by treatment with 50% fetal bovine serum for 2 h. Cells were then washed and returned to complete culture medium; the end of serum shock was defined as CT0. Independent culture wells were collected at CT0, CT2, CT4, CT6, CT8, CT10, CT12, CT14, CT16, CT18, CT20, CT22, and CT24. Three biologically independent BMDM preparations were analyzed at each time point, and the same culture well was not sampled repeatedly.

Clock and *Piezo1* expression were normalized to 18S rRNA. The $2^{-\Delta Ct}$ values were used for circadian analysis without separately rescaling the CT0 value of each genotype, thereby preserving differences in overall expression levels between $Clock^{fl/fl}$ and $Clock^{\Delta LysM}$ BMDMs. Rhythmic expression was assessed using a Cosinor model with a fixed period of 24 h to estimate the mesor and amplitude.

S20. Fibroblast contraction, migration, and mechanical assays

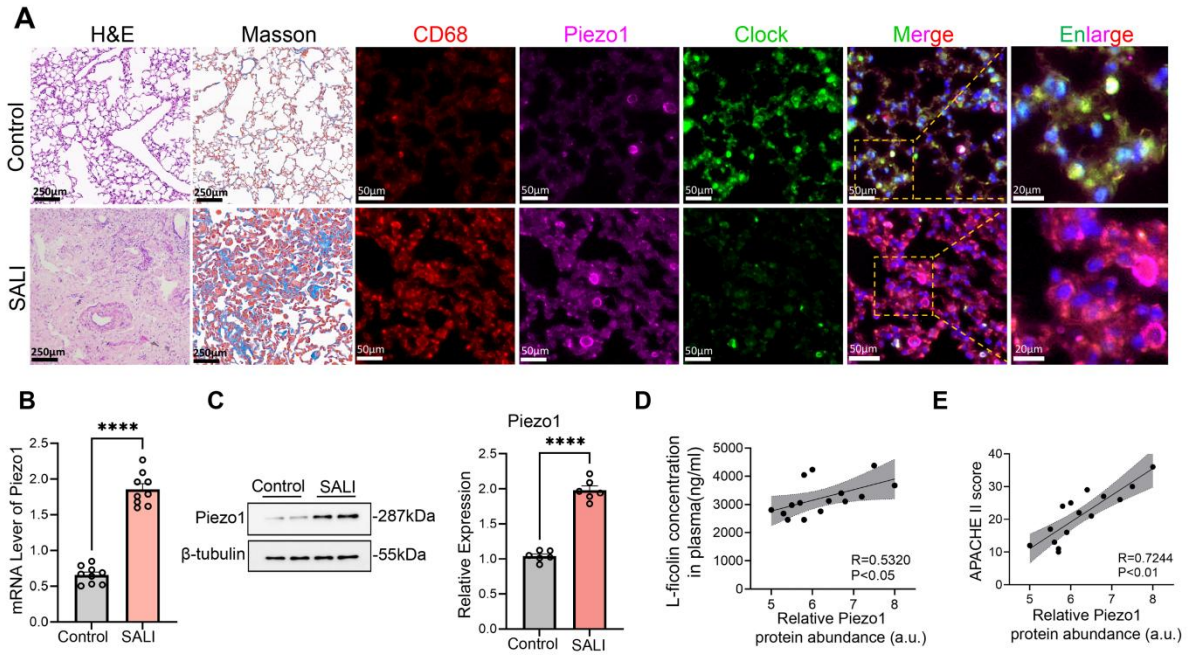
For collagen-gel contraction assays, primary lung fibroblasts were embedded in type I collagen gels at a final collagen concentration of 2.0 mg/mL. After gel release, contraction was recorded over 24 h and expressed relative to the initial gel size. For Transwell migration assays, pretreated BMDMs were washed and placed in the lower chamber, whereas lung fibroblasts were seeded into 8-μm pore inserts. After migration, cells on the lower membrane surface were fixed, stained with crystal violet, and quantified. For scratch closure assays, confluent fibroblast monolayers were scratched, washed, and incubated with macrophage-derived conditioned signals. Images were acquired at 0, 12 and 24 h, and scratch closure was quantified in ImageJ. For p-MLC

imaging, fibroblasts were stained with anti-phospho-MLC (Ser19), and representative fluorescence images were acquired under identical imaging settings across groups. For atomic force microscopy, macrophages and fibroblasts were co-cultured on glass-bottom dishes and analyzed using a silicon nitride cantilever with a nominal spring constant of approximately 0.03 N/m. Topographic and stiffness maps were generated, and apparent Young's modulus was calculated using the Hertz model.

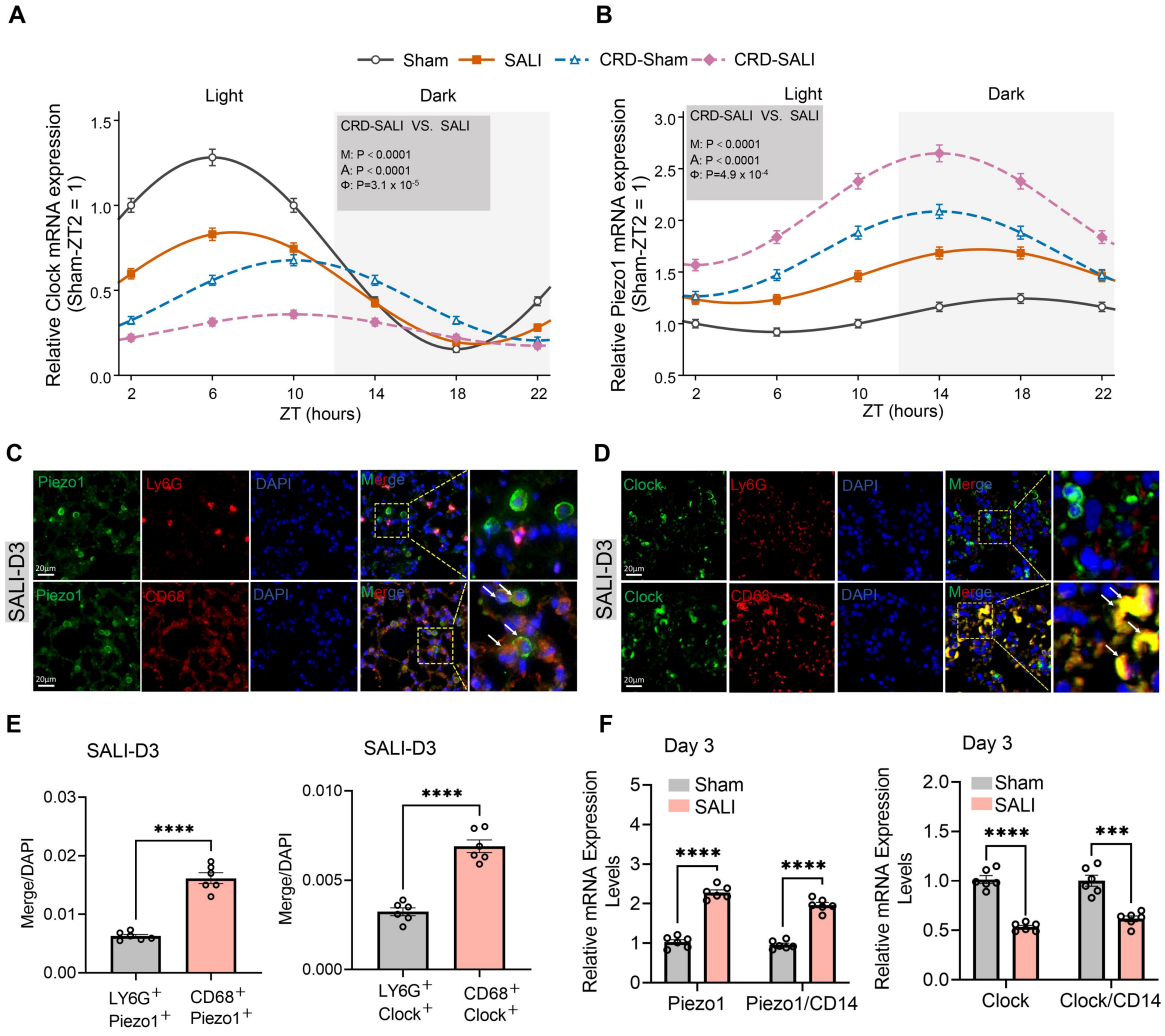
S21. Single-cell expression analysis for Figure 1, A and B

The expression analyses of *Piezo1* and *Clock* in Figure 1, A and B used Sham and CLP 24-h lung samples from GSE207651. Each sequencing library was generated from lung tissues pooled from three mice. Macrophage-lineage, epithelial and fibroblast populations were selected using the existing cell-type annotations. Within each cell, each gene count was divided by the total count across genes, multiplied by 10,000 and transformed using ln(1 + x). Figure 1A shows the per-cell distribution of log1p-normalized expression across lung cell populations. Figure 1B compares expression between Sham and CLP 24-h samples within each selected cell population. For Figure 1B, the arithmetic mean of these values was calculated across all cells within each cell type and condition, including cells with zero expression. Dot colors represent the resulting mean log1p-normalized expression; dot sizes represent the percentage of cells with an expression value > 0. Neither Z-score transformation nor gene-wise scaling was applied.

Supplemental Figure legends



Supplemental Figure S1. Clinical lung-tissue validation of PIEZO1 and CLOCK expression. (A) Representative H&E and Masson's trichrome staining and human lung immunofluorescence (CD68, red; PIEZO1, magenta; CLOCK, green; DAPI, blue). Scale bars: 250 μm (histology), 50 μm (immunofluorescence), 20 μm (magnified views). **(B,C)** Human lung *PIEZO1* mRNA by RT–qPCR **(B)** and PIEZO1 protein by immunoblotting and densitometry **(C)**. **(D,E)** Correlations of relative lung PIEZO1 protein abundance with plasma L-ficolin **(D)** or APACHE II score **(E)** in 15 SALI patients. PIEZO1 was normalized to membrane-matched β-tubulin and a pooled reference lysate common to all membranes. For A, n = 5 participants/group; for B, n = 9 participants/group; for C, n = 6 measurements/group. Cohort characteristics and analysis-specific sample sizes are in Supplemental Table 1. Data are mean ± SEM; B,C, unpaired two-tailed Student's t test; D,E, Pearson correlation with linear regression. ns, not significant; *$P < 0.05$, **$P < 0.01$, ***$P < 0.001$, ****$P < 0.0001$.



283

284 **Supplemental Figure S2. Four-group circadian profiling and cell localization of pulmonary CLOCK and**

285 **PIEZO1 following septic lung injury and circadian disruption. (A,B)** Relative mRNA expression of *Clock*

286 **(A)** and *Piezo1* **(B)** in lung tissues from Sham, SALI, CRD－Sham and CRD－SALI mice sampled at ZT2, ZT6,

287 ZT10, ZT14, ZT18 and ZT22 on postoperative day 3. Expression was normalized to *Gapdh*, and the mean value

288 of the Sham－ZT2 group was used as the common calibrator and assigned a value of 1. Points show mean ± SD;

289 n = 6 biologically independent mice per group at each time point. Curves show joint linear Cosinor fits with

290 a fixed 24-h period, and the shaded region denotes the dark phase (ZT12－ZT24). M, mesor; A, amplitude; Φ,

291 acrophase. *P* values shown in the insets are two-sided Holm-adjusted pairwise comparisons of the corresponding

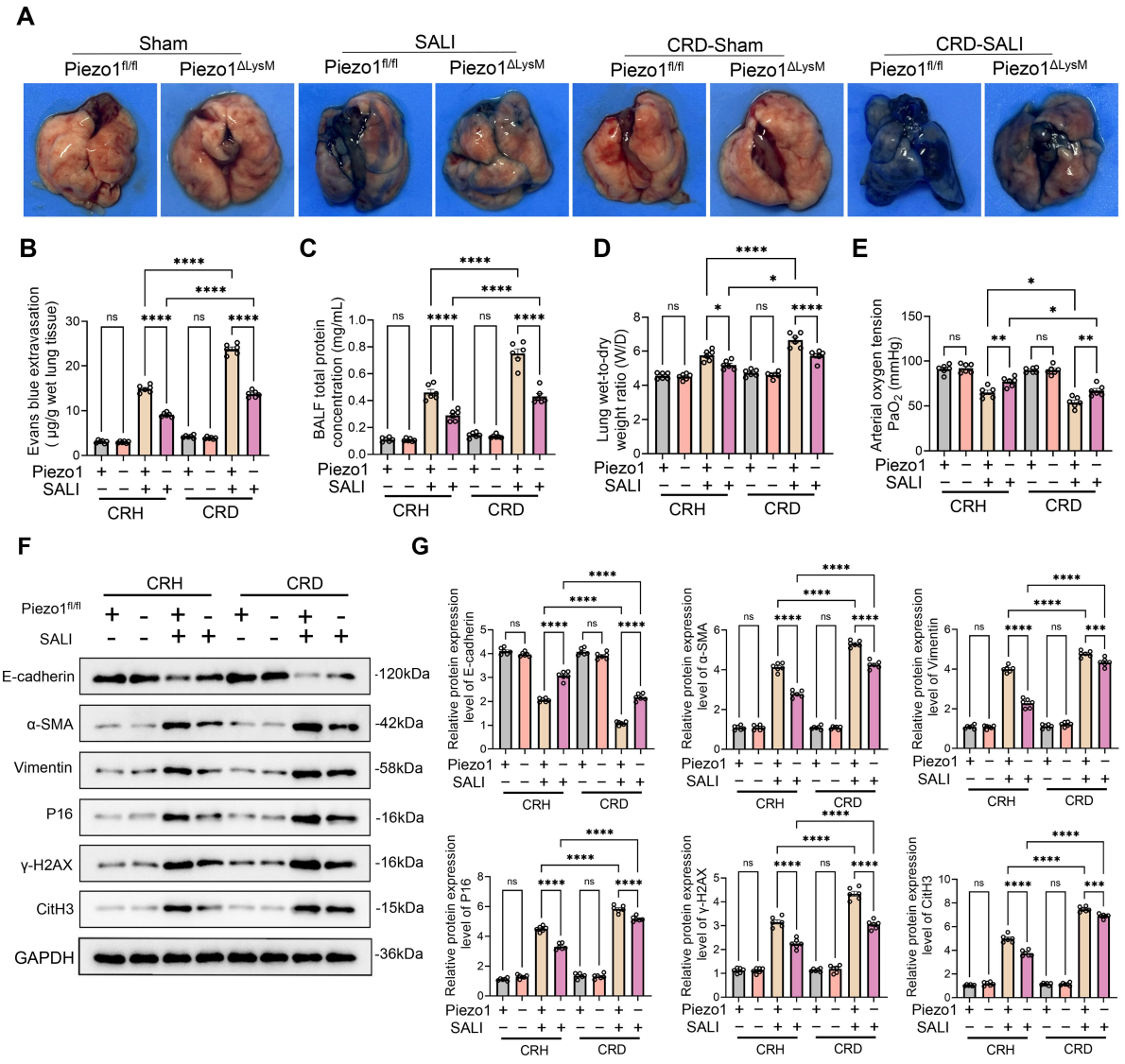
292 Cosinor parameters between the CRD－SALI and SALI groups. In the prespecified factorial Cosinor analysis,

293 the CRD－SALI interaction was significant for *Clock* amplitude (*P = 0.0036*) and *Piezo1* acrophase (*P =*

294 *0.0337*), whereas interactions for the remaining Cosinor parameters were not significant. **(C-E)** PIEZO1 or

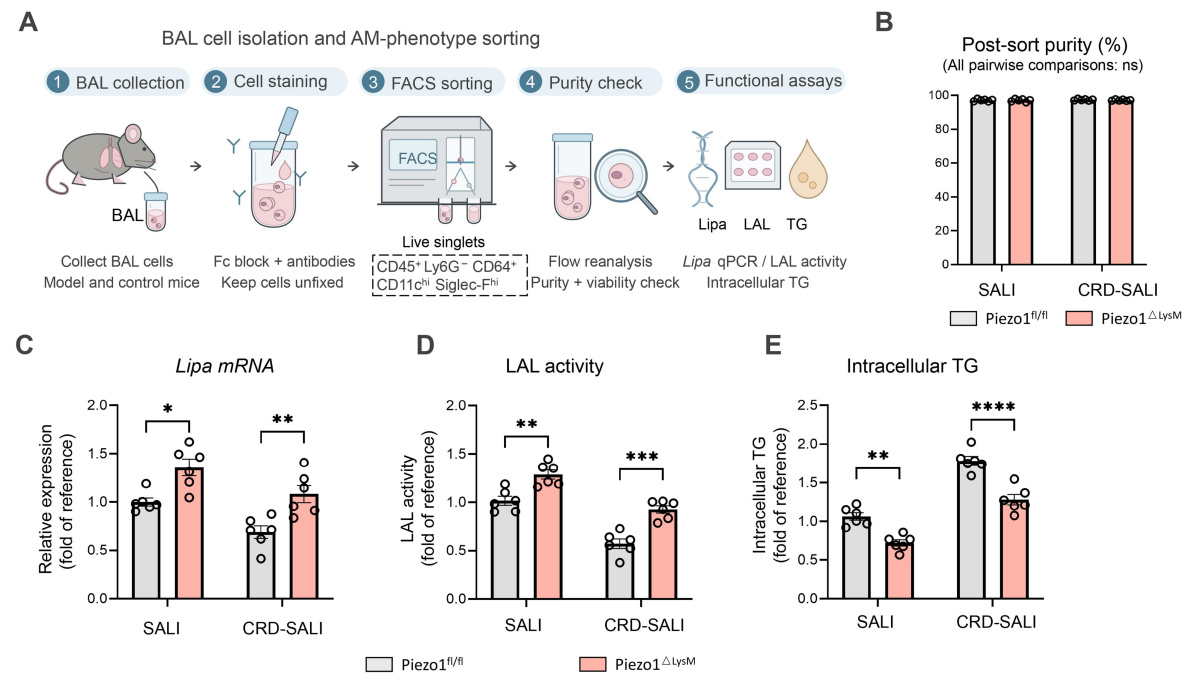
295 CLOCK localization (green) in Ly6G$^+$ neutrophils (red, upper) versus CD68$^+$ macrophages (red, lower) **(C,D)**,

with Merge/DAPI quantification on postoperative day 3 **(E)**. Arrows indicate colocalization; scale bar, 20 μm. **(F)** RT-qPCR analysis of lung tissues collected in this study from Sham and SALI mice on postoperative day 3. Expression is shown before and after additional *Cd14* normalization, with *Gapdh* as the reference gene and Sham as the calibrator. E,F: n = 6 biologically independent mice per group; mean ± SEM. E, unpaired two-tailed Student's t test; F, two-way ANOVA with Sidak's test. ns, not significant; *$P < 0.05$, **$P < 0.01$, ***$P < 0.001$, ****$P < 0.0001$.



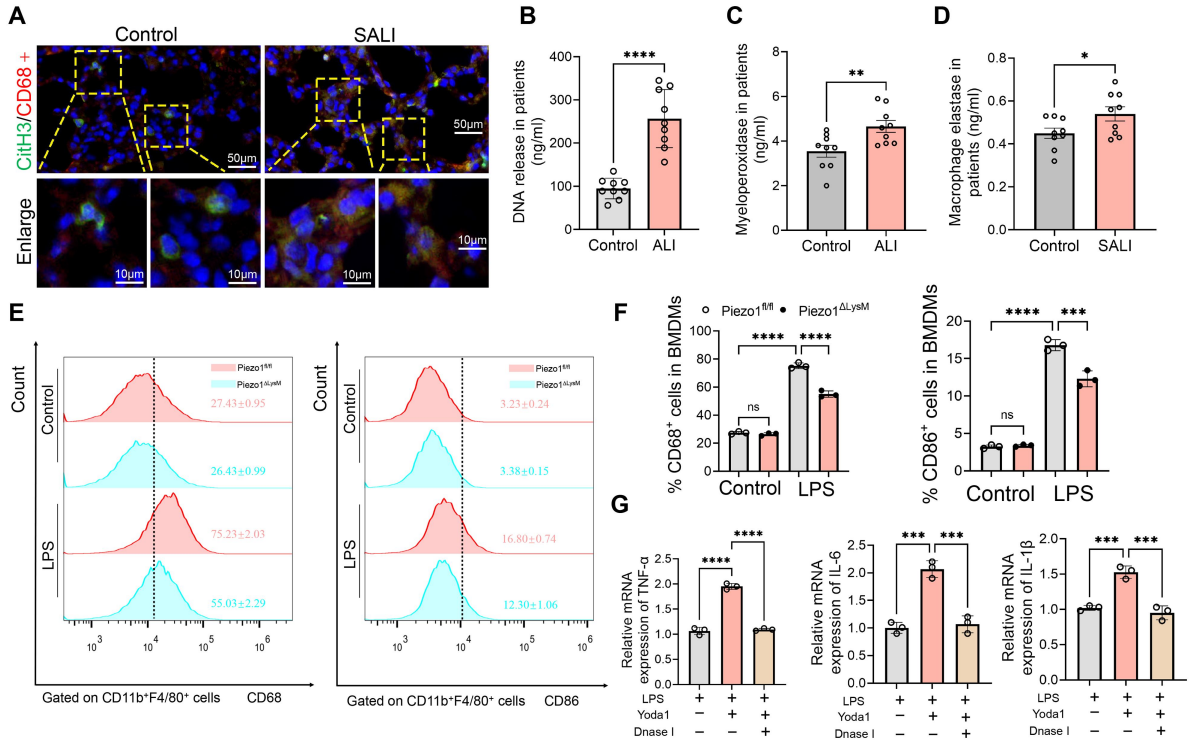
Supplemental Figure S3. Early pulmonary barrier dysfunction, edema, impaired oxygenation and late remodeling after single-hit CLP. (A) Representative whole-lung images following Evans blue administration in Sham, SALI, CRD–Sham, and CRD–SALI mice with the indicated *Piezo1* genotypes. **(B)** Quantification of

Evans blue extravasation in lung tissue. **(C)** Total protein concentration in bronchoalveolar lavage fluid. **(D)** Lung wet-to-dry weight ratio. **(E)** Arterial oxygen tension (PaO_2) measured in blood collected from the left common carotid artery of spontaneously breathing mice under 1.5% isoflurane anesthesia in room air. A–E were assessed on postoperative day 3. **(F,G)** Day-28 lung immunoblots **(F)** and densitometry of EMT markers (E-cadherin, α-SMA, vimentin), senescence/damage markers (p16, γ-H2AX) and CitH3-positive extracellular-trap-associated signals **(G)**. Each target was normalized to membrane-matched GAPDH from the same samples and lane set; one representative GAPDH row is shown, and complete controls are provided with the uncropped immunoblots. n = 6 biologically independent mice per group (each point, one mouse); representative panels A and F derive from the corresponding cohorts. Data are mean ± SD **(B–E)** or SEM **(G)**. B–E,G, three-way ANOVA (circadian condition, injury and genotype) followed by Sidak's multiple-comparison test. ns, not significant; *$P < 0.05$, **$P < 0.01$, ***$P < 0.001$, ****$P < 0.0001$.

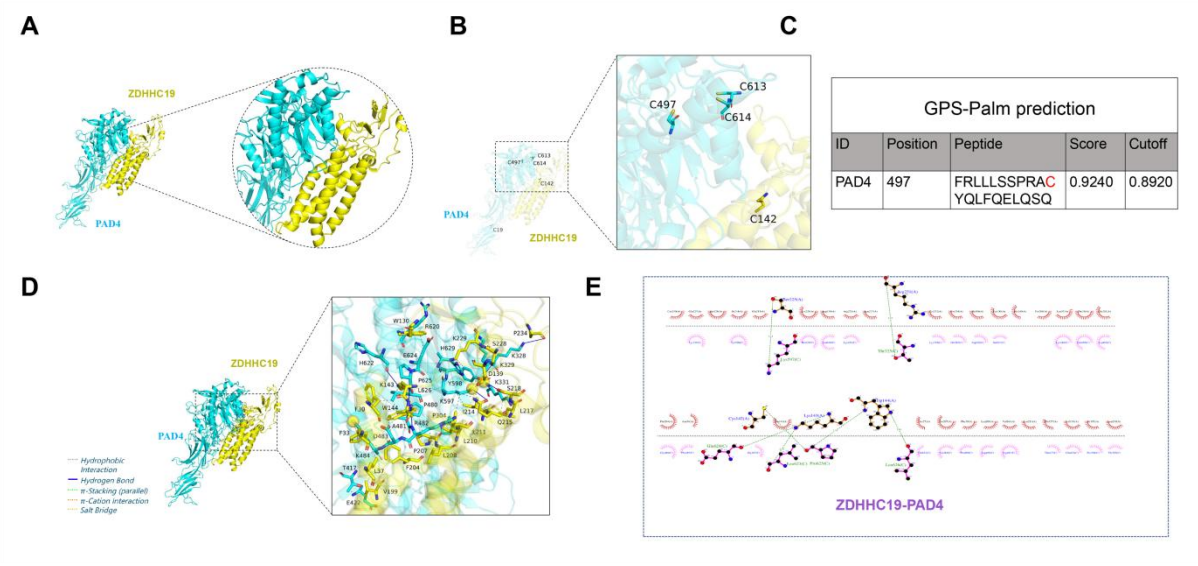


Supplemental Figure S4. Ex vivo metabolic validation in alveolar macrophages from SALI and CRD–SALI mice. (A) Bronchoalveolar lavage (BAL) collection, live-cell sorting and post-sort reanalysis. Alveolar macrophages (AMs) were gated as live singlet $CD45^+Ly6G^-CD64^+CD11c^{hi}Siglec\text{-}F^{hi}$ cells. **(B)** Post-sort purity; all pairwise comparisons were nonsignificant. **(C–E)** *Lipa* mRNA **(C)**, lysosomal acid lipase (LAL) activity **(D)** and intracellular triglycerides (TG; **E**) in *Piezo1*$^{fl/fl}$ and *Piezo1*$^{\Delta LysM}$ AMs under SALI or CRD–SALI conditions, expressed relative to the SALI *Piezo1*$^{fl/fl}$ reference. n = 6 preparations/group; each point

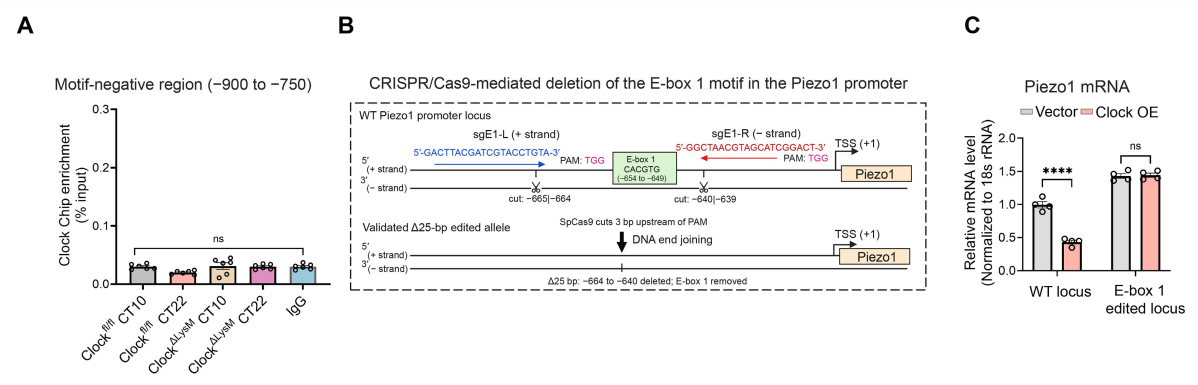
represents one preparation. Data are mean ± SEM. B, one-way ANOVA with Tukey's multiple-comparison test. C–E, two-way ANOVA with genotype and CRD status as factors, including their interaction, followed by Sidak's multiple-comparison test to compare genotypes within each condition and conditions within each genotype. For C, statistical analyses were performed on ΔCt values. ns, not significant; *$P < 0.05$, **$P < 0.01$, ***$P < 0.001$, ****$P < 0.0001$.



Supplemental Figure S5. Clinical extracellular-trap markers and additional macrophage inflammatory analyses. (A) Representative lung immunofluorescence from controls and patients with septic lung injury for CitH3 (green), CD68 (red) and DAPI (blue); yellow boxes indicate enlarged colocalization. Scale bars, 50 μm (main) and 10 μm (enlarged). **(B–D)** Serum cell-free DNA **(B)**, MPO **(C)** and macrophage elastase **(D)** in controls and patients with septic lung injury (n = 9 per group; mean ± SEM). **(E,F)** Representative flow-cytometry histograms **(E)** and percentages of $CD68^+$ and $CD86^+$ cells among $CD11b^+F4/80^+$ BMDMs **(F)**. **(G)** Cytokine mRNA after LPS, Yoda1 and/or DNase I. For A, n = 6 independent staining experiments; for E–G, n = 3 independently prepared BMDM cultures per group. Data are mean ± SEM; B–D, unpaired two-tailed Student's t test; F,G, one-way ANOVA with Tukey's post hoc test. ns, not significant; *$P < 0.05$, **$P < 0.01$, ***$P < 0.001$, ****$P < 0.0001$.

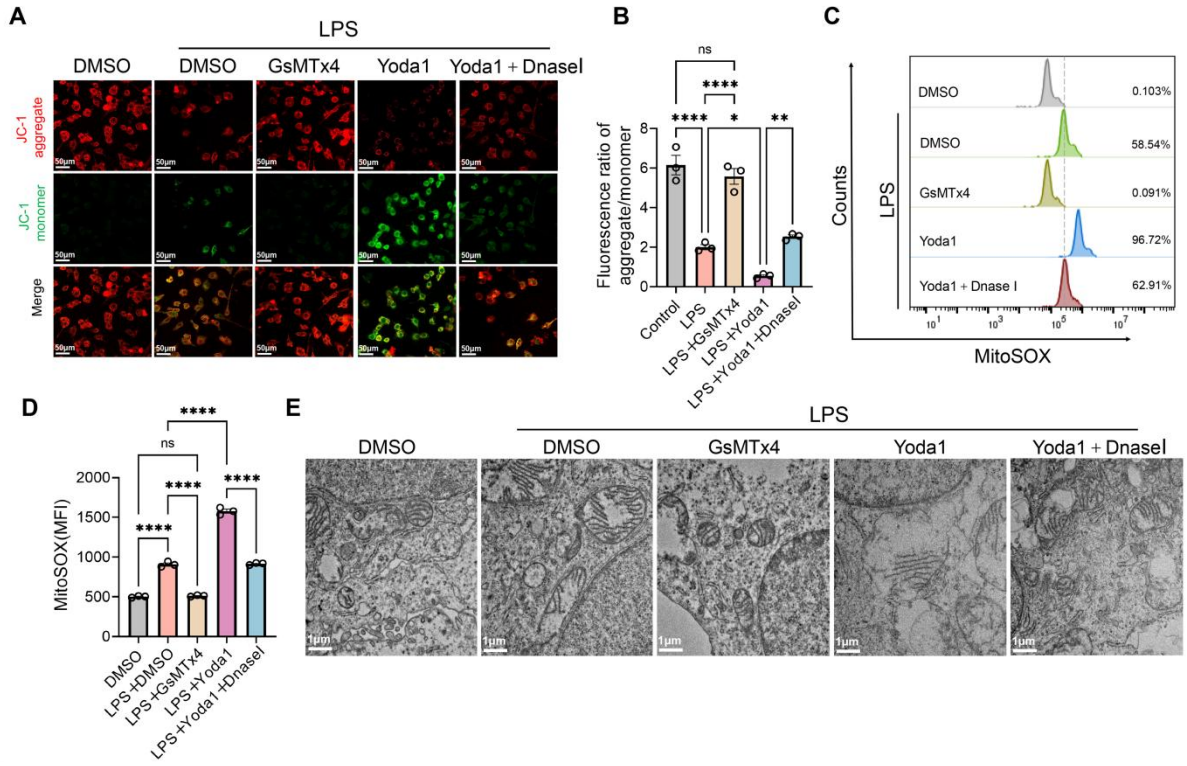


Supplemental Figure S6. Structural modeling and S-palmitoylation-site mapping of the ZDHHC19–PAD4 complex. (A,B,D,E) Structural modeling of the ZDHHC19-PAD4 complex. **(A)** Overview of the docked complex. **(B)** Zoomed-in view showing the catalytic site of ZDHHC19 adjacent to PAD4-C497. **(C)** GPS-Palm prediction of PAD4 S-palmitoylation at Cys497 (prediction score, 0.9240; high-stringency cutoff, 0.8920). **(D)** Detailed interface interactions. **(E)** 2D interaction map.

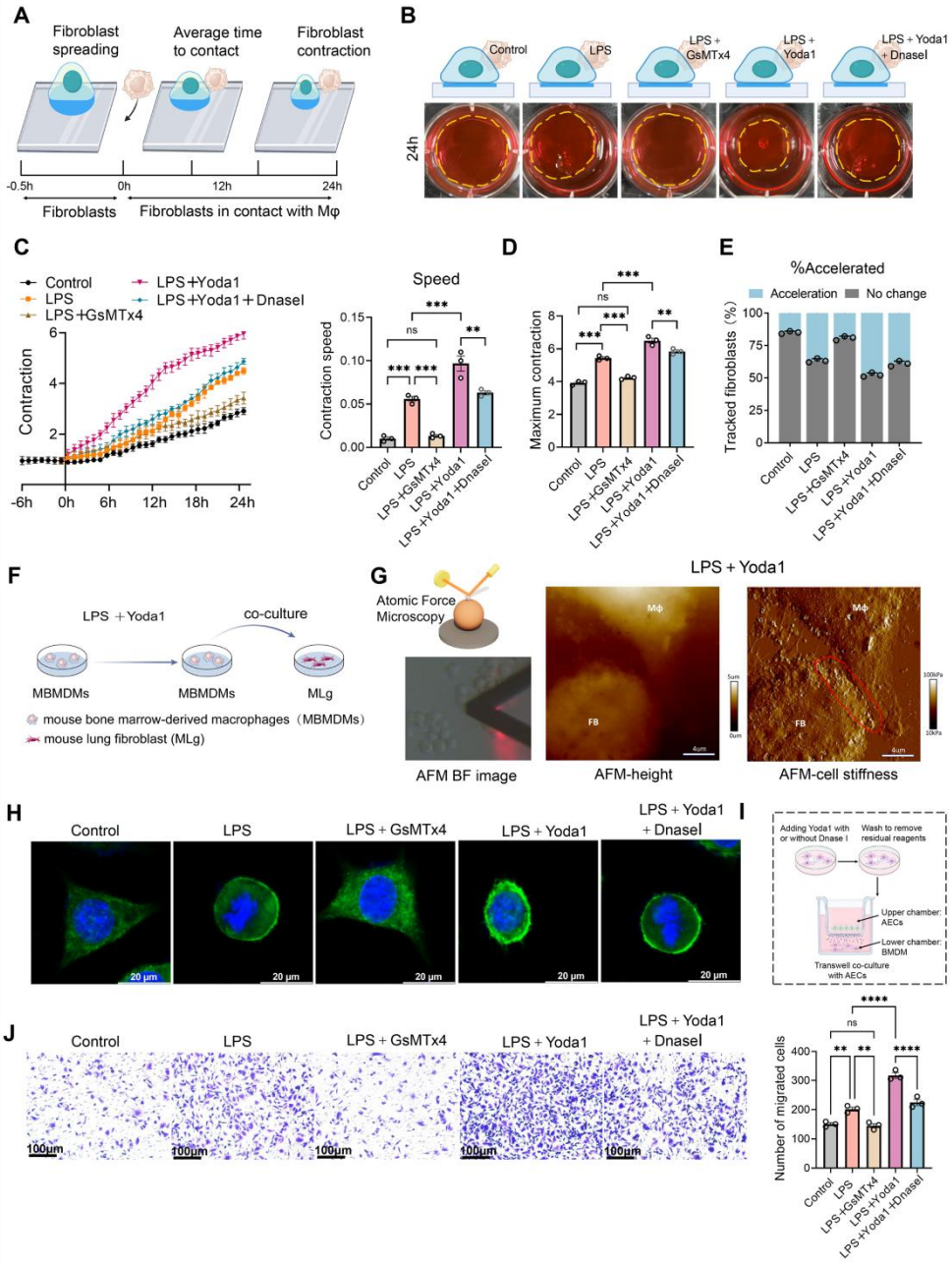


Supplemental Figure S7. Controls and endogenous editing for CLOCK-dependent *Piezo1* regulation. (A) ChIP-qPCR enrichment at the motif-negative region (−900 to −750 bp), expressed as percentage input. **(B)** Paired-sgRNA deletion of endogenous E-box 1, showing protospacers, PAMs, SpCas9 cleavage sites and the validated 25-bp deletion (−664 to −640 bp). **(C)** 18S rRNA-normalized *Piezo1* mRNA in wild-type or E-box-edited BMDMs with vector or CLOCK overexpression. For A, n = 6 independently prepared cultures per group; for C, n = 4. Data are mean ± SEM. Two-way ANOVA with Sidak's test was used for A and C, with genotype, circadian time, locus or CLOCK overexpression as appropriate; IgG in A was a background control,

not a factor level. All tests were two-sided. ns, not significant; *$P < 0.05$; **$P < 0.01$; ***$P < 0.001$; ****$P < 0.0001$.

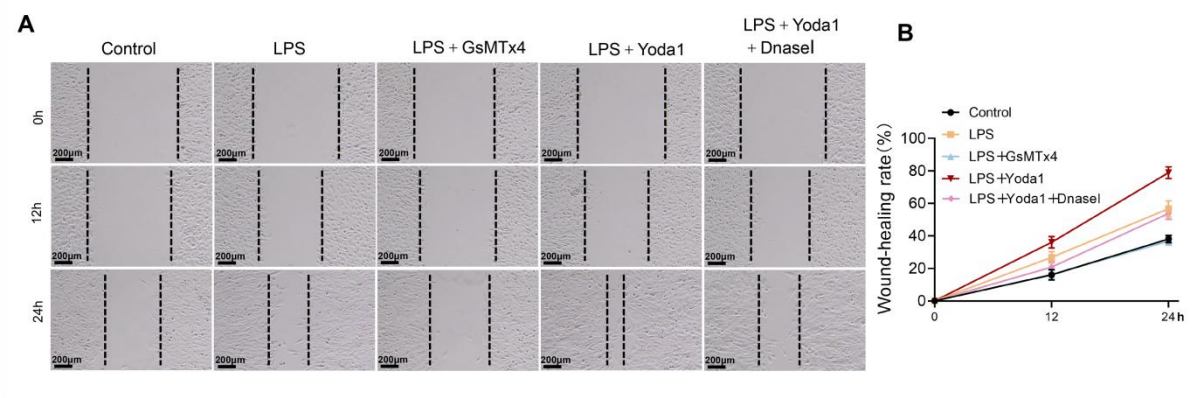


Supplemental Figure S8. AEC mitochondrial function and ultrastructure after exposure to macrophage-derived MET-like signals. (A–D) AEC mitochondrial function assessed by JC-1 membrane-potential imaging **(A,B)** and MitoSOX flow cytometry **(C,D)**; GsMTx4 or DNase I provided rescue. **(E)** Transmission electron microscopy showing cristae rupture and vacuolization. For B,D, n = 3 independently prepared BMDM–AEC co-cultures per group; representative TEM in E was repeated in 6 independent experiments. Data are mean ± SEM; B,D, one-way ANOVA with Tukey's post hoc test. ns, not significant; *$P < 0.05$, **$P < 0.01$, ***$P < 0.001$, ****$P < 0.0001$.



Supplemental Figure S9. PIEZO1-enhanced macrophage-associated METs promote fibroblast contraction, mechanical stress and migration under septic-like conditions. (A–E) Collagen-gel contraction assay: schematic **(A)**, representative gels at 24 h (B; smaller area indicates greater contraction), 24-h contraction kinetics and speed **(C)**, maximum contraction **(D)**, and proportion of accelerated events **(E)**. **(F–H)** Direct macrophage–fibroblast co-culture: schematic **(F)**; representative bright-field image, AFM height map and apparent Young's modulus map at the macrophage–fibroblast interface under LPS + Yoda1 (G; scale bar, 4 μm); and fibroblast p-MLC immunofluorescence showing actomyosin organization (H; p-MLC, green; DAPI, blue; scale bar, 20 μm). **(I,J)** Transwell migration assay: pretreated BMDMs were washed and placed in the lower

chamber, with lung fibroblasts in the upper insert **(I)**; representative crystal-violet staining and migrated-cell quantification (J; scale bar, 100 μm). For C–E, and J, n = 3 independent experiments per group; for G, n = 6. Data are mean ± SD. C, two-way repeated-measures ANOVA with Sidak's multiple-comparisons test; D, E, and J, one-way ANOVA with Tukey's post hoc test. ns, not significant; **P < 0.05; **P < 0.01; ***P < 0.001; ****P < 0.0001.*



Supplemental Figure S10. Fibroblast scratch closure after exposure to BMDM-conditioned medium. (A,B) Representative images **(A)** and quantification **(B)** of fibroblast scratch closure at 0, 12 and 24 h after exposure to BMDM-conditioned medium; scale bar, 200 μm. n = 3 independent experiments per group. Data are mean ± SD. B, two-way repeated-measures ANOVA with Sidak's multiple-comparisons test. ns, not significant; **P < 0.05; **P < 0.01; ***P < 0.001; ****P < 0.0001.*

Supplemental Table 1. Demographic and clinical characteristics of the human lung-tissue cohort and sample availability for Supplemental Figure S1

Characteristic or analysis	Non-injured controls (n = 15)	SALI (n = 15)	Complete cases, n	*P* value or statistical result
Demographic characteristics				
Age, years	55.1 ± 9.7	57.8 ± 10.6	30	0.473
Male sex, n (%)	9 (60.0)	10 (66.7)	30	1.000
Body mass index, kg m^{-2}	23.6 ± 2.7	24.1 ± 3.0	30	0.635
Smoking status, n (%)			30	0.875
Never	8 (53.3)	7 (46.7)		
Former	5 (33.3)	5 (33.3)		
Current	2 (13.3)	3 (20.0)		
Specimen characteristics				
Tissue source, n (%)			30	1.000

Characteristic or analysis	Non-injured controls (n = 15)	SALI (n = 15)	Complete cases, n	*P* value or statistical result
Organ-donor lung tissue	12 (80.0)	11 (73.3)		
Surgical or explant lung tissue	3 (20.0)	4 (26.7)		
Time from tissue acquisition to preservation, min	27 [22–34]	29 [23–36]	30	0.589
Comorbidities				
Hypertension, n (%)	5 (33.3)	6 (40.0)	30	1.000
Diabetes mellitus, n (%)	2 (13.3)	3 (20.0)	30	1.000
Cardiovascular disease, n (%)	2 (13.3)	3 (20.0)	30	1.000
Chronic pulmonary disease, n (%)	1 (6.7)	2 (13.3)	30	1.000
Chronic kidney disease, n (%)	1 (6.7)	2 (13.3)	30	1.000
Clinical characteristics at sampling				
Pulmonary infection, n (%)	0 (0)	11 (73.3)	30	<0.001
APACHE II score	NA	23.9 ± 6.2	15	NA
SOFA score	NA	10.3 ± 3.1	15	NA
PaO_2/FiO_2, mmHg	NA	148 [112–186]	15	NA
Invasive mechanical ventilation, n (%)	NA	13 (86.7)	15	NA
Vasopressor treatment, n (%)	NA	12 (80.0)	15	NA
Time from SALI diagnosis to sampling, days	NA	2 [1–3]	15	NA
Plasma L-ficolin, ng ml^{-1}	2,760 ± 410	3,420 ± 620	30	0.002
Primary source of infection in patients with SALI				
Pulmonary, n (%)	NA	10 (66.7)	15	NA
Abdominal, n (%)	NA	3 (20.0)	15	NA
Urinary tract, n (%)	NA	1 (6.7)	15	NA
Other, n (%)	NA	1 (6.7)	15	NA
Availability of samples for Supplemental Figure S1, A–E				
Histology and immunofluorescence, Supplemental Figure S1A	5	5	10	Representative
Lung-tissue RT–qPCR, Supplemental Figure S1B	9	9	18	Group comparison
Lung-tissue immunoblotting, Supplemental Figure S1C	6	6	12	Group comparison
Matched lung PIEZO1 and plasma L-ficolin, Supplemental Figure S1D	NA	15	15 pairs	r = 0.5320; *P < 0.05*
Matched lung PIEZO1 and APACHE II score, Supplemental Figure S1E	NA	15	15 pairs	r = 0.7244; *P < 0.01*

Note: Data are mean ± SD, median [interquartile range] or n (%), as appropriate. Continuous variables were compared using two-sided Welch's t-tests or Mann–Whitney U-tests, according to data distribution. Categorical variables were compared using two-sided Fisher's exact tests or Pearson's χ^2-tests. No imputation was performed; each analysis used samples with complete data for the variables concerned. The group-comparison immunoblotting in Supplemental Figure S1C represents the molecular-validation subset, whereas Supplemental Figure S1, D and E used the clinical-correlation subset with matched lung-tissue and clinical measurements.

Abbreviations: APACHE II, Acute Physiology and Chronic Health Evaluation II; SALI, sepsis-associated lung injury; SOFA, Sequential Organ Failure Assessment; NA, not applicable.

Supplemental Table 2. Primers used in the study

Target (Gene)	Forward primer (5′-3′)	Reverse primer (5′-3′)
Piezo1	TTCTTCGGGTTGGAGAGGTA	TGTCACCATGTGGTTAAGGATG
Clock	GAGAGCGCGAAGGAAATCT	CCAATCAACAACGCCTGTAA
Bmal1	ACCTCGCAGAATGTCACAGGCA	CTGAACCATCGACTTCGTAGCG
Nr1d1	TCCAGTACAAACGGTGTCTGAAA	GCCAACGGAGAGACACTTCTTG
Cd14	TCTACCGACCATGGAGCGT	CCGCCGTACAATTCCACA
Tnf	TCTTCTCATTCCTGCTTGTGG	ATGAGAGGGAGGCCATTTG
Il1b	GCAACTGTTCCTGAACTCAACT	ATCTTTTGGGGTCCGTCAACT
Il6	CAAAGCCAGAGTCCTTCAGAG	AGCATTGGAAATTGGGGTAG
Ulk1	AAGCACGATTTGGAGGTCGC	TGATTTCCTTCCCCAGCAGC
Cpt1a	GGTCTTCTCGGGTCGAAAGC	TCCTCCCACCAGTCACTCAC
Hadh	ACTACATCAAAATGGGCTCTCAG	AGCAGAAATGGAATGCGGACC
Acaca	GATGAACCATCTCCGTTGGC	GACCCAATTATGAATCGGGAGTG
Gapdh	CCCTTAAGAGGGATGCTGCC	GTTCACACCGACCTTCACCA
18S rRNA	CCTTGGATGTGCTGCCTT	GCGGCTTTGGTGACTCTA

Supplemental Table 3. Antibody sources, catalog numbers and dilutions

Target	Dilution	Manufacturer	Catalog no. / clone
PIEZO1	1:1,000	Abcam	ab259949; EPR23826-103
REV-ERBα	1:1,000	Cell Signaling Technology	13418; E1Y6D
BMAL1	1:1,000	Abcam	ab3350; polyclonal
CLOCK	1:1,000	Abcam	ab3517; polyclonal
Citrullinated Histone H3 (CitH3)	1:1,000	Abcam	ab5103; polyclonal
MPO	1:1,000	Proteintech	66177-1-Ig; 4C11F6
MMP-2	1:1,000	Abcam	ab92536; EPR1184
MMP-9	1:1,000	Cell Signaling Technology	3852; polyclonal
MMP-12	1:500–1:1,000	Proteintech	22989-1-AP; polyclonal
PAD4 (PADI4)	1:1,000	Abcam	ab128086; OTI4H5
ZDHHC19 (DHHC19)	1:1,000	Abcam	ab179545; polyclonal
LC3B	1:1,000	Cell Signaling Technology	2775; polyclonal
p62 / SQSTM1	1:1,000	Abcam	ab109012; EPR4844

Target	Dilution	Manufacturer	Catalog no. / clone
LAL	1:1,000	Abcam	ab154356; polyclonal
ULK1	1:1,000	ABclonal	A8529;polyclonal
CPT1A	1:1,000	Abcam	ab128568; 8F6AE9
HADH	1:1,000	Proteintech	19828-1-AP; polyclonal
ACACA / ACC1	1:1,000	Cell Signaling Technology	3662; polyclonal
α-SMA	1:1,000–1:2,000	Abcam	ab7817; 1A4
E-cadherin	1:1,000	Abcam	ab15148; polyclonal
Vimentin	1:1,000	Abcam	ab92547; EPR3776
γ-H2AX	1:1,000	ABclonal	AP0099; polyclonal
β-actin (loading control)	1:5,000	Sigma-Aldrich	A5441; AC-15
β-tubulin (loading control)	1:5,000	Abcam	ab6046; polyclonal
GAPDH	WB 1:20,000	Abcam	ab8245; 6C5
p16INK4a	WB 1:1,000; IF 1:100	Abcam	ab211542; EPR20418
LAMP1	IF 1:200	Cell Signaling Technology	9091; D2D11
p-MLC (Ser19)	IF 1:50	Cell Signaling Technology	3671; polyclonal
CD45 (mouse flow)	Flow 1:200	BioLegend	103138; 30-F11; BV510
Ly6G (mouse flow)	Flow 1:200	BioLegend	127624; 1A8; APC-Cy7
CD64 (mouse flow)	Flow 1:200	BioLegend	139314; X54-5/7.1; PE-Cy7
CD11c (mouse flow)	Flow 1:200	BioLegend	117310; N418; APC
Siglec-F (mouse flow)	Flow 1:200	BD Biosciences	552126; E50-2440; PE
CD11b (mouse flow)	Flow 1:100	BD Biosciences	553310; M1/70; FITC
F4/80 (mouse)	Flow 1:100	BioLegend	123110; BM8; PE
CD86 (mouse flow)	Flow 1:100	BioLegend	105006; GL-1; FITC
CD206 (mouse flow)	Flow 1:200	BioLegend	141720; C068C2; PE-Cy7
CD68 (mouse flow)	Flow 0.5 μg/10^6 cells	Thermo Fisher Scientific	25-0681-82; FA-11; PE-Cy7
CD68 (mouse tissue)	IF 1:100	Abcam	ab125212; polyclonal
CD68 (human tissue)	IF 1:100	Abcam	ab955; KP1
CD16/CD32 (Fc block)	1 μg/10^6 cells	BD Biosciences	553141; 2.4G2
Flag tag	WB 1:1,000	Sigma-Aldrich	F1804; M2

Target	Dilution	Manufacturer	Catalog no. / clone
SFB-tag detection via S-tag	WB 1:5,000	MilliporeSigma/Novagen	71549; S-Tag monoclonal; detects the S-tag component
ChIP control IgG	Same antibody mass as anti-CLOCK	Cell Signaling Technology	3900; DA1E; rabbit IgG
Anti-rabbit IgG–HRP	WB 1:2,000	Cell Signaling Technology	7074; polyclonal
Anti-mouse IgG–HRP	WB 1:2,000	Cell Signaling Technology	7076; polyclonal
Anti-rabbit IgG–Alexa Fluor 488	IF 1:500	Abcam	ab150077; polyclonal
Anti-mouse IgG–Alexa Fluor 488	IF 1:500	Abcam	ab150117; polyclonal
Anti-rat IgG–Alexa Fluor 594	IF 1:500	Abcam	ab150160; polyclonal
Anti-rabbit IgG–Alexa Fluor 594	IF 1:500	Abcam	ab150080; polyclonal
Anti-mouse IgG–Alexa Fluor 594	IF 1:500	Abcam	ab150120; polyclonal
Anti-rabbit IgG–Alexa Fluor 647	IF 1:500	Abcam	ab150079; polyclonal
Anti-mouse IgG–Alexa Fluor 647	IF 1:500	Abcam	ab150119; polyclonal

Flow-cytometry dilutions were based on approximately 10^6 cells in 100 µL. AM sorting and macrophage profiling used separate panels. WB, immunoblotting; IF, immunofluorescence.